Title: Sonochemical Fabrication of Cu(II) and Zn(II) Metal-Organic Framework Films on Metal Substrates

Article Type: Full Length Article

Corresponding Author: Professor Seonghwan Kim, Ph.D.

Corresponding Author's Institution: University of Calgary

First Author: Osama Abuzalat

Order of Authors: Osama Abuzalat; Danny Wong; Mohamed Elsayed, Ph.D.; Simon Park, Ph.D.; Seonghwan Kim, Ph.D.

Abstract: In this article, we demonstrate a rapid and facile method for in-situ growth of metal-organic framework (MOF) films on Cu or Zn metal substrates by sonochemical techniques. The substrates were first treated with a strong oxidizing agent to convert the metal to the corresponding metal hydroxide. Ultrasonic irradiation provided the energy to drive the reaction between the metal ion sources and organic ligands. Four MOF films (Cu-BTC, Cu-BDC, ZIF-8 and MOF-5) were successfully fabricated by this approach. The produced films were characterized by scanning electron microscopy and x-ray diffraction analysis. The effects of organic ligand concentration and ultrasonic irradiation time on MOF film synthesis were also systematically investigated. The rapid and facile fabrication method presented in this article could serve a new route to grow MOF films on various gas sensor surfaces. Of the MOF films, ZIF-8 film was tested as a potential methane sensor.

Highlights

- Cu-BTC, Cu-BDC, ZIF-8 and MOF-5 films are synthesized successfully on metal substrates by a rapid and facile sonochemical method.

- The MOFs films show good crystallinity, homogeneity, and adhesion to the metal substrates.

- Sonochemically synthesized ZIF-8 film is chosen to test the feasibility of our method in gas sensing applications. ZIF-8 film shows good responses to different methane concentrations

Sonochemical Fabrication of Cu(II) and Zn(II) Metal-Organic Framework Films on Metal Substrates

Osama Abuzalat[1], Danny Wong[1], Mohamed Elsayed[1,2], Simon Park[1], Seonghwan Kim[1,*]

[1]Department of Mechanical and Manufacturing Engineering, University of Calgary, Calgary, Alberta

T2N 1N4, Canada

[2]Department of Chemical Engineering, Military Technical College, Cairo, Egypt

Abstract

In this article, we demonstrate a rapid and facile method for in-situ growth of metal-organic framework (MOF) films on Cu or Zn metal substrates by sonochemical techniques. The substrates were first treated with a strong oxidizing agent to convert the metal to the corresponding metal hydroxide. Ultrasonic irradiation provided the energy to drive the reaction between the metal ion sources and organic ligands. Four MOF films (Cu-BTC, Cu-BDC, ZIF-8 and MOF-5) were successfully fabricated by this approach. The produced films were characterized by scanning electron microscopy and x-ray diffraction analysis. The effects of organic ligand concentration and ultrasonic irradiation time on MOF film synthesis were also systematically investigated. The rapid and facile fabrication method presented in this article could serve a new route to grow MOF films on various gas sensor surfaces. Of the MOF films, ZIF-8 film was tested as a potential methane sensor.

Keywords: sonochemistry, metal-organic frameworks, surface modification, methane sensor

*Corresponding author e-mail: sskim@ucalgary.ca; address: 2500 University Drive NW, Calgary, Alberta, Canada T2N 1N4 office ICT 251

1. Introduction

Porous coordination polymers, also known as metal-organic frameworks (MOFs), are one-, two-, or three-dimensional crystalline structure materials consisting of metal cluster nodes and organic linkers, which have uncommonly large surface areas [1, 2]. By rational selection of appropriate synthesis conditions with nodes and linkers, it is possible to produce MOFs of desired surface area, pore size, functionality, and topology [3]. Recently, the field of MOFs in chemistry is developing at a rapid pace with an increase in the number of published papers and reviews appearing in the literature [4-7]. MOFs have shown potential applications in gas storage and separation [8-10], catalysis [11, 12], ion exchange [13], and gas sensing [14-16]. Crystal growth techniques such as slow diffusion, layering solutions, hydrothermal methods and solvothermal methods are usually used to synthesize crystalline porous MOFs [17-19]. In the conventional synthesis route, a mother solution containing metal salts are prepared in a capped autoclave with different concentrations of organic linkers; the solution is then heated at a determined temperature for a certain duration. Then the solid product is recovered by filtration or centrifugation. Parameters such as solvent selection, temperature, pH, organic ligand concentration, synthesis time, and even anion types are found to be major factors affecting the formation of MOFs [20].

Recently, many alternative synthesis techniques have been investigated where energy is provided through microwave irradiation [21, 22], electrical potential (electrochemistry) [23, 24], mechanical excitation (mechanochemistry) [4, 25], and ultrasound (sonochemistry) [26, 27]. Sonochemistry is a phenomenon in which the reaction mixture undergoes a chemical change upon application of high-energy ultrasound irradiation from 20 kHz to 10 MHz [24, 28]. The details of sonochemistry including ultrasound power, temperature, reaction time, and their applications can be found in many publications [29-31]. When passing through the reaction mixture, ultrasound irradiation can generate homogenous nucleation centers that lead to decreased MOF crystallization time compared with classic solvothermal or hydrothermal

techniques [32, 33]. Son et al. reported successful preparation of high-quality MOF-5 crystals of 5–25 µm in size via a sonochemical method in considerably reduced time (ca. 30 min) compared to conventional solvothermal methods (24 h) [26]. In another report, Jung et al. used a low-cost solvent (1-methyl-2-pyrrolidone, called NMP) for successful fabrication of high-quality MOF-177 crystals (size range of 5–20 µm) in 40 min via a sonochemical route [34]. Moreover, MOF-177 was produced under similar conditions (35 min, size range of 5–50 µm) using microwave heating in NMP but exhibited lower crystallinity. In contrast, a traditional solvothermal preparation route took approximately 48 h to produce MOF-177 crystals (size range of 0.5–1.5 mm) in diethylformamide [35]. Kim et al. investigated a novel sonochemical route for controlling the arrangement of CuTATB-n MOFs by adjusting the ultrasonic power levels, and studied its effect on CO_2 adsorption [36].

Even though many MOFs crystals have been synthesized by a sonochemical method, there have been limited reports on the sonochemical fabrication of MOF films on metal substrates. In this paper, we demonstrate a rapid and facile fabrication of MOF films on metal substrates using a two-step sonochemical approach. The effects of sonication time and organic linker concentrations on the MOF film morphologies were systematically investigated. In addition, to prove the versatility of this method, four well-known MOF compounds (Cu-BTC, Cu-BDC, ZIF-8, and MOF-5) were synthesized on either a Cu or Zn substrate and characterized by scanning electron microscopy (SEM) and x-ray diffraction (XRD) techniques.

The rapid and facile method presented in this article could serve a new route to grow MOF films on various gas sensor surfaces. Thus, to show a feasibility of sonochemically synthesized MOF film-based gas sensor, ZIF-8 film on a metal substrate was tested and demonstrated as a potential methane sensor.

2. Experimental Details

2.1 Materials

Trimesic acid (1, 3, 5-benzenetricarboxylic acid [H$_3$BTC, 98 %, Alfa Aesar]), terephthalic acid (benzene-1, 4-dicarboxylic acid [BDC, 98+ %, VWR]), 2-methylimidazole (2-MIM, 99 %, Aldrich), N,N-dimethylformamide (DMF, 99.8 %, VWR), triethylamine (TEA, 99 %, Alfa Aesar), ammonium persulfate ((NH$_4$)$_2$S$_2$O$_8$, 98 %, Aldrich), acetone (ACE, 99 %, VWR), and distilled deionized water (DDW) were used without further purification in the synthesis of MOF films. Copper-clad substrate (RS component code: 159–5773) and zinc strip (0.25 mm thick, 99.98 %, Alfa Aesar) were used as substrates in the MOF film syntheses.

2.2 Metal substrate preparation

Cu-BTC and Cu-BDC were synthesized on a copper-clad substrate, and ZIF-8 and MOF-5 films were synthesized on a commercial zinc strip. Prior to synthesis of the MOF films on the metal substrate, the substrates were sonicated for 20 min in a 1:1 mixture of ethanol and DDW to remove any contaminants on the surfaces. After being washed with copious amounts of DDW and ACE, the substrates were dried with nitrogen. After the metal substrates were cleaned, the metallic copper and zinc substrates were immersed into an aqueous solution of 4 ml sodium hydroxide (NaOH, 10M), 2 ml ammonium persulfate ((NH$_4$)$_2$S$_2$O$_8$, 1M), and 9 ml DDW. Cu(OH)$_2$ nanotubes and Zn(OH)$_2$ nanostrands [37] were formed after 30 min and 60 min of oxidation, respectively.

2.3 Preparation of precursor solutions and synthesis of MOF films

For the preparation of Cu-BTC films, BTC (0.1 mM, 0.5 mM, 3 mM) were dissolved in 5 ml of DMF. For Cu-BDC and MOF-5 films, the precursor solution was prepared by dissolving BDC (0.5 mM, 1 mM, 3 mM) in 11 ml of DMF. For ZIF-8 films, 2-MIM (0.05 mM, 0.1 mM, 0.5 mM) were dissolved in 100 ml of DDW and 10.1 ml of TEA. After stirring the precursor solutions vigorously for about 10 min, the metal

hydroxide substrates were immersed in the corresponding precursor solutions and then sonicated at room temperature for times varying from 5 min to 60 min. A sonicator (GemOro, Richmond, VA) with a frequency of 40 kHz and an ultrasonic power of 100 watts was used because it provided sufficient energy for MOF film formation. The temperature gradually increased with increasing sonication time. The starting temperature was 22 °C and increased to 25 °C, 30 °C, 35 °C, and 45 °C at intervals of 5, 15, 30, and 60 min, respectively. After the fabrication of MOF films, the substrates were washed with copious amounts of DDW and ACE, and dried with nitrogen.

2.4 Characterization

A field emission scanning electron microscope (FE-SEM, QuantaTM 250) was used to investigate and analyze the morphologies and an x-ray diffractomer (XRD, Rigaku Multiflex) was utilized to characterize the crystalline structure of the two metal hydroxide and four MOFs films. Adhesion tests of four MOFs films were performed by tape test according to ASTM D3359-02 [38] and by a sonication method [39] .

3. Results and discussion

3.1 Selection of a substrate and surface modification

Adhesion, anchoring, and nucleation of MOF crystals to substrates depend on the structure and chemical constitution of the substrate surface. Utilizing a metal substrate to act as a metal ion source facilitates the formation of a thin MOF film. When the substrate is a metal such as Cu or Zn, the in-situ growth of the MOF film can be more effective, because the metal substrate may act as a source of metal ions for the synthesis of the MOF film [40]. Furthermore, the organic ligand can be easily combined with dissolved metal ions on the metal substrate to form well-defined MOF structures. The binding strength of the linker molecules mainly depends on the acid/base properties of the substrate surfaces. Moreover, some metal

oxide surfaces can form strong covalent bonds with carboxylic acids and therefore offer the anchoring of carboxylic acid-based MOFs [41]. Figure 1 illustrates the two-step method for the rapid and facile synthesis of MOF films on metal substrates. Oxidation of the metal surfaces to metal hydroxides facilitates the liberation of metal ions over the surface [42]. The use of high-intensity ultrasound enhances the dissolution rate of metal ions from the metal hydroxide. This facilitate the coordination with organic ligands ions to form MOF networks [43]. Figure 2 (a) and (b) show that the copper surface has been converted to copper hydroxide nanowires and that the zinc surface has been converted to zinc hydroxide nanostrands after metal substrate oxidation step.

XRD was used to confirm the conversion from metal (Cu and Zn) to the corresponding metal hydroxides. Figure 3 (a) and (b) show that new peaks have appeared after oxidation of the metal substrate, which represents conversion of pure metal to metal hydroxide. In the case of copper shown in Figure 3 (a), three new peaks at $2\theta = 16.9°$, $24.02°$, and $34.28°$ appeared after oxidation, which correspond to (020), (021), and (002), respectively, for $Cu(OH)_2$ [44]. Four new peaks also appeared for the Zn metal substrate as shown in Figure 3 (b) at $2\theta = 21.6°$, $32.38°$, $35°$, and $48.1°$, which correspond to (101), (100), (002), and (112), respectively, for $Zn(OH)_2$ [45, 46].

3.2 Synthesis of copper-based MOF films: Cu-BTC and Cu-BDC

The primary mechanism in sonochemical synthesis is acoustic cavitation. The creation, growth, and collapse of bubbles in the liquid generate extremely high local temperatures (5000–25000 K) and pressures, and lead to rapid releases of energy [26]. The corresponding solid surfaces are cleaned, eroded, or activated to promote chemical reactions under the high energy and intense shear force [47]. In this work, the high transient temperature plays a major role in the reaction between the metal ion and organic ligands [26]. Without ultrasonic irradiation, no MOFs were obtained under the same synthesis condition (data not shown). First, the effects of varying ultrasonic irradiation time from 5 min to 60 min were

6

studied using SEM and XRD. As shown in Figures 4 (a) and 4 (e), both Cu-BTC and Cu-BDC films were synthesized after just 5 min of ultrasonic irradiation. The ordinary octahedral cubic structure of Cu-BTC was produced, and the rod structure of Cu-BDC with crystal size less than 500 nm was generated. In addition, we noticed that by increasing the sonication time, the shape of the crystal became more defined and well developed as shown in Figures 4 (b–d) and 4 (f–h). This effect was most evident after 30 min of sonication. After examining and analyzing the SEM images of these samples, the crystal size of Cu-BTC seems to increase as a function of ultrasonic irradiation time, and the same trend can be noticed with Cu-BDC nanorods (see supplementary section S1). This size change is commonly observed in sonochemical synthesis due to an increase in the crystallization and growth rate during the in-situ growth [26, 48].

Figure 5 (a) and (b) show the XRD patterns, which confirm that Cu-BTC and Cu-BDC crystals have been formed on the Cu metal substrate. At longer reaction time, strong peaks with higher intensity were observed. Distinct peaks at 2θ = 6.82˚, 9.64˚, and 11.74˚, which correspond to (200), (220), and (222), respectively, suggest the formation of a thin Cu-BTC film [40]. For Cu-BDC, the peaks appear at 2θ = 7.8˚ and 17.6˚, which correspond to (001) and (002), respectively [49]. The intensity of the peaks increased with longer sonication time until a maximum intensity was reached at 30 min. This might be due to the complete conversion of all available metal ions on the corresponding metal hydroxide layer.

3.3 Synthesis of zinc-based MOF films: ZIF-8 and MOF-5

Figures 6 (a–d) show the growth of ZIF-8 crystals on oxidized Zn metal substrates as a function of sonication time. The crystals have rough surfaces, but some angles could be observed. The shapes varied from cubes exposing 6 faces to intermediate shapes to parallelograms exposing 12 faces. The 12-face parallelogram could be considered the most stable equilibrium morphology of ZIF-8. The oxidation of zinc metal to zinc hydroxide allowed many Zn^{2+} ions to be available for reaction with the 2-MIM linkers. Confined ZIF-8 crystals with an average size of approximately 500 nm could be noticed after only 5 min

of ultrasonic irradiation, but the ZIF-8 film is mainly composed of aggregates containing crystals with poorly resolved shapes. As seen in Figures 6 (a–d), ZIF-8 crystal growth occurred when increasing the reaction time to 30 min and 60 min. SEM images of the MOF-5 as a function of sonication time are shown in Figure 6 (e–h). After 5 min of sonication, as shown in Figure 6 (e), MOF-5 was formed in spherical shapes composed of agglomerated sponge-type crystals. This deterioration in the crystal quality seems to occur due to the decay of the organic ligand in the crystallized MOF-5 [50]. Excess zinc clusters, formed on the surface, may also compete for organic ligand in the MOF-5 crystals already formed. However, further increases in sonication time, shown in Figures 6 (f–h), seem to enhance uniformity and particle definition. We analyzed the SEM images to determine the effect of increasing sonication time on the crystal size. Contrary to the other three MOFs produced, MOF-5 had a decreasing average crystal size with increasing sonication time. This is likely due to the complex formation of several nuclei resulting in a decrease in crystal size.

X-ray diffraction patterns in Figure 7 (a) demonstrate that pure ZIF-8 phase is formed on the zinc metal substrate. The comparative intensities and notable peak positions at 2θ = 7.7˚, 10.7˚, 13˚, 18˚, 18.5˚, 27˚, and 30˚ correspond to (011), (002), (112), (013), (222), (233), and (044), respectively. This is in good agreement with previous reports [47, 51-53]. The results showed that, with the increased sonication time, the peaks became more sharp and intense. However, a slight peak shift was noticed on ZIF-8 XRD patterns. Strain resulting from prolonged irradiation of ultrasonic waves is very likely to occur in a thin film. Peaks will typically shift to lower angle with compressive stress and to higher angle with tensile stress [54].

Figure 7 (b), shows the XRD pattern of prepared MOF-5 at different sonication time. the appearance of four peaks at 2θ = 9.2˚, 14.8˚, 16.1˚, and 17.8˚, which correspond to (220), (400), (420), and (440), respectively, suggest that the formation of MOF-5 films were achieved [26, 55] even at 5 min sonication.

The peak strength also increased with increasing the sonication time as we observed in other MOF film cases.

3.4 Effect of different concentration of organic ligands on MOFs synthesis

The crystalline structure and morphology of the synthesized MOFs are greatly affected by the concentration of organic ligands and the deprotonation rate. The rapid and facile synthesis of the four MOF films was systematically studied as a function of organic ligand concentrations. All MOF films used for studying the effect of organic ligand concentration were prepared using 5 min ultrasonic irradiation. Figure 8 shows the XRD patterns of the four MOF films at different concentrations of organic ligands. At 3 mM of BTC organic ligand concentration, almost no Cu-BTC crystals were observed with SEM (see supplementary section S2). We noticed an amorphous phase over the hydroxide layer; consequently, no peaks of either Cu-BTC nor $Cu(OH)_2$ were observed in the XRD pattern as shown in Figure 8 (a). At this high concentration, not all organic ligands were dissolved; consequently, the solution was very turbid, and the undissolved organic ligands may prevent dissolved ones from diffusion towards Cu ions causing the reaction to be very slow. This behavior may be changed if we change the solvent used in this study. In contrast, for the 0.5 mM of BTC solution condition, well-defined cubic crystals of Cu-BTC were clearly observed (see Figure 4 (a)). In addition, a lower concentration of organic ligand (0.1 mM of BTC) also resulted in the formation of Cu-BTC with some well-defined cubic structures. However, the surface density and homogeneity of the crystals are not as good as Cu-BTC crystals with 0.5 mM of BTC (see supplementary section S2). For Cu-BDC, the rod structure was well observed at the concentration of 1 mM of BDC, which was confirmed by SEM (see supplementary section S2) and the XRD pattern in Figure 8 (b). However, at a lower concentration of BDC (0.5 mM), an amorphous phase was observed with very few Cu-BDC crystals formed. Moreover, we noticed trace amounts of $Cu(OH)_2$ nanowires in the SEM images (see supplementary section S2). This suggests insufficient organic ligand ions exist to

crystallize and form well-developed Cu-BDC crystals. At a higher concentration of BDC (3 mM), even though some nanorods of Cu-BDC crystals were observed, the Cu-BDC film lacks surface density and homogeneity. In addition, we noticed residues of unreacted $Cu(OH)_2$ nanowires in the SEM images (see supplementary section S2). This is also reflected on the XRD pattern showing a peak at $2\theta = 24.02°$ in Figure 8 (b).

Figure 8 (c) shows the XRD patterns of ZIF-8 films at different organic ligand concentrations. Crystals of ZIF-8 with well-defined edges were observed at 0.05 mM of 2-MIM. However, the surface density and homogeneity of the film was low (see supplementary section S2). At 0.1 mM of 2-MIM, a highly dense film of ZIF-8 crystals was observed (see Figure 6 (a)). By increasing the concentration of 2-MIM up to 0.5 mM, we could still observe a highly dense film with larger ZIF-8 crystals (see supplementary section S2). This may be due to the high solubility of the 2-MIM organic ligand in polar solvents even at high concentrations. The dissolution rate of organic ligands seems to be sufficient to form well-developed ZIF-8 crystals.

For MOF-5 preparations at 0.5 mM of BDC, the MOF-5 crystals were much smaller than those obtained with 1 mM of BDC (see supplementary section S2). Even though MOF-5 crystals were observed with SEM, these small crystals were not detected with XRD as shown in Figure 8 (d). By increasing the concentration of BDC up to 1 mM, we could observe larger MOF-5 crystals with SEM (see Figure 6 (e)) and confirm the formation of a MOF-5 film with the XRD pattern in Figure 7 (b) and 8 (d). In addition, larger crystals with defects were observed at 3 mM of BDC (see supplementary section S2). This was reflected in the XRD pattern, shown in Figure 8 (d), where a very sharp peak with high intensity at $2\theta = 9.1°$ was noticed alongside new peaks at $2\theta = 17.3°, 25.2°, 25.7°,$ and $28.1°$. It seems that aggregation of BDC organic ligand molecules has occurred at higher concentrations.

3.5 Adhesion tests of the MOF films

Strong adhesion of a MOF film at the interface between the film and the metal substrate is important especially in gas sensing applications. We tested the adhesion of the four MOF films by tape test according to ASTM D3359-02 [38] and by a sonication method [39]. Four MOF films, Cu-BTC with 0.5 mM BTC, Cu-BDC with 1 mM BDC, ZIF-8 with 0.1 mM 2-MIM, and MOF-5 with 1 mM BDC, were prepared by the method stated above with 5 min of ultrasonic irradiation. Standard tape tests were performed according to ASTM D3359 by applying and removing pressure sensitive tape over cuts made in the MOF films. SEM images show that the films have good adhesion as most crystals are still attached to the substrate after tape test (see supplementary section S3). In addition, ultrasonic tests were performed by placing four MOF films separately in vials containing ethanol. Then they were sonicated in an ultrasonic bath (40 kHz and ultrasonic power of 100 watts) for up to 60 min. SEM images in Figure 9 show that the films have good adhesion as most crystals remain still attached to the substrate after 60 min of sonication. Minimal changes to MOF films occurred at time intervals of 5, 10, 30, and 60 min.

3.6 Methane sensing potential of ZIF-8 film

ZIF-8 film on a Zn substrate was employed to demonstrate the feasibility of sonochemically synthesized MOF film-based gas sensor. ZIF-8 is commonly used for methane storage and separation due to excellent molecular sieving properties [37]. The framework's structural flexibility, via a swing effect in the imidazole linkers, allows the adsorption of methane (kinetic diameter ~ 0.38 nm) even into the smaller secondary pores (average pore size ~0.34 nm) [53, 56]. Furthermore, it has been shown that ZIF-8 is selective to methane because it is more permeable to smaller molecules such as H_2, CO_2, O_2 and N_2 [53]. Potentio electrical impedance spectroscopy (PEIS) was utilized to show methane sensing potential of ZIF-8 film. Setup for gas sensing experiments is well described in supplementary information section S4. Figure 10 shows the results from running PEIS on the ZIF-8 film after it was exposed to different methane concentrations. The results show that the total impedance decreases as the injected methane

concentration increases and low frequencies result in larger responses. At frequencies, f, above 100,000 Hz, the responses are almost negligible. The largest sensor responses ($\Delta R/R_a$), 26.4%, 24.0%, and 15.1%, were obtained at 3600 Hz for 375 ppm, at 1.98 Hz for 250 ppm and at 27.3 Hz for 125 ppm, respectively. These sensor responses suggest that ZIF-8 films may be feasible as a methane sensing material with low frequency impedance measurements.

4. Conclusion

In summary, four well-known MOFs were synthesized as films over a metal substrate by a rapid and facile sonochemical method. The process is simple, straight-forward, and has yet to be reported. The sonication time and organic ligand concentrations are crucial factors. The crystal size increased with prolonged exposure to the ultrasonic irradiation except in the MOF-5 film. The use of high-intensity ultrasound enhanced the reactivity of metal hydroxide and the organic linker. This led to an increase in the crystallization and growth rate during the in-situ growth for Cu-BTC, Cu-BDC, and ZIF-8. The optimal concentrations of organic ligands are 0.5 mM BTC for Cu-BTC; 0.1 mM 2-MIM for ZIF-8; and 1 mM BDC for MOF-5 and Cu-BDC. The films were fully converted and homogeneous at these concentrations. Utilizing the metal hydroxide to act as the metal ion source facilitated the formation of good MOF films with strong bonding with the metal substrate. This method is expected to be useful in the preparation of other MOF films such as MOF-74, IRMOF-62, MIL-101, and MOF-199.

It was also shown that the sonochemically synthesized ZIF-8 film exhibited noticeable responses to methane gas. The sensor showed potential in differentiating various concentrations of methane. Future works will look to expand on the gas sensing performance of the synthesized MOFs. The selectivity of the MOF film gas sensors will be tested using different gases.

Acknowledgments

Appendix A. Supplementary data

Supplementary data associated with this article can be found, in the online version, at [link]

References

1. Biradha, K., A. Ramanan, and J.J. Vittal, *Coordination polymers versus metal– organic frameworks.* Crystal Growth and Design, 2009. **9**(7): p. 2969-2970.
2. Kitagawa, S., R. Kitaura, and S.i. Noro, *Functional porous coordination polymers.* Angewandte Chemie International Edition, 2004. **43**(18): p. 2334-2375.
3. MacGillivray, L.R. and C.M. Lukehart, *Metal-Organic Framework Materials*. 2014: Wiley.
4. Cliffe, M.J., et al., *Accelerated aging: a low energy, solvent-free alternative to solvothermal and mechanochemical synthesis of metal–organic materials.* Chemical Science, 2012. **3**(8): p. 2495-2500.
5. Rosi, N.L., et al., *Advances in the chemistry of metal-organic frameworks.* CrystEngComm, 2002. **4**(68): p. 401-404.
6. Küsgens, P., et al., *Characterization of metal-organic frameworks by water adsorption.* Microporous and Mesoporous Materials, 2009. **120**(3): p. 325-330.
7. Kaye, S.S., et al., *Impact of preparation and handling on the hydrogen storage properties of Zn4O (1, 4-benzenedicarboxylate) 3 (MOF-5).* Journal of the American Chemical Society, 2007. **129**(46): p. 14176-14177.
8. Britt, D., D. Tranchemontagne, and O.M. Yaghi, *Metal-organic frameworks with high capacity and selectivity for harmful gases.* Proceedings of the National Academy of Sciences, 2008. **105**(33): p. 11623-11627.
9. Farrusseng, D., *Metal-organic frameworks: applications from catalysis to gas storage*. 2011: John Wiley & Sons.
10. Li, J.-R., J. Sculley, and H.-C. Zhou, *Metal–organic frameworks for separations.* Chemical reviews, 2011. **112**(2): p. 869-932.
11. Lee, J., et al., *Metal–organic framework materials as catalysts.* Chemical Society Reviews, 2009. **38**(5): p. 1450-1459.
12. Farrusseng, D., S. Aguado, and C. Pinel, *Metal–organic frameworks: opportunities for catalysis.* Angewandte Chemie International Edition, 2009. **48**(41): p. 7502-7513.
13. MacGillivray, L.R., *Metal-Organic Frameworks: Design and Application*. 2010: Wiley.

14.   Lu, G. and J.T. Hupp, *Metal– organic frameworks as sensors: a ZIF-8 based Fabry– Pérot device as a selective sensor for chemical vapors and gases.* Journal of the American Chemical Society, 2010. **132**(23): p. 7832-7833.

15.   Kreno, L.E., et al., *Metal–organic framework materials as chemical sensors.* Chemical reviews, 2011. **112**(2): p. 1105-1125.

16.   Schröder, M., *Functional Metal-Organic Frameworks: Gas Storage, Separation and Catalysis*. Vol. 293. 2010: Springer.

17.   Zhou, H.-C., J.R. Long, and O.M. Yaghi, *Introduction to metal–organic frameworks*. 2012, ACS Publications.

18.   Mueller, U., et al., *Metal–organic frameworks—prospective industrial applications.* Journal of Materials Chemistry, 2006. **16**(7): p. 626-636.

19.   Ahrenholtz, S.R., C.C. Epley, and A.J. Morris, *Solvothermal preparation of an electrocatalytic metalloporphyrin MOF thin film and its redox hopping charge-transfer mechanism.* Journal of the American Chemical Society, 2014. **136**(6): p. 2464-2472.

20.   Rowsell, J.L. and O.M. Yaghi, *Metal–organic frameworks: a new class of porous materials.* Microporous and Mesoporous Materials, 2004. **73**(1): p. 3-14.

21.   Choi, J.-S., et al., *Metal–organic framework MOF-5 prepared by microwave heating: factors to be considered.* Microporous and Mesoporous Materials, 2008. **116**(1): p. 727-731.

22.   Yoo, Y., Z. Lai, and H.-K. Jeong, *Fabrication of MOF-5 membranes using microwave-induced rapid seeding and solvothermal secondary growth.* Microporous and Mesoporous Materials, 2009. **123**(1): p. 100-106.

23.   Martinez Joaristi, A., et al., *Electrochemical synthesis of some archetypical Zn2+, Cu2+, and Al3+ metal organic frameworks.* Crystal Growth & Design, 2012. **12**(7): p. 3489-3498.

24.   Ameloot, R., et al., *Patterned growth of metal-organic framework coatings by electrochemical synthesis.* Chemistry of Materials, 2009. **21**(13): p. 2580-2582.

25.   James, S.L., et al., *Mechanochemistry: opportunities for new and cleaner synthesis.* Chemical Society Reviews, 2012. **41**(1): p. 413-447.

26.   Son, W.-J., et al., *Sonochemical synthesis of MOF-5.* Chemical Communications, 2008(47): p. 6336-6338.

27.   Zeng, X., et al., *Sonocrystallization of ZIF-8 on electrostatic spinning TiO2 nanofibers surface with enhanced photocatalysis property through synergistic effect.* ACS Applied Materials & Interfaces, 2016. **8**(31): p. 20274-20282.

28.   Schoedel, A., C. Scherb, and T. Bein, *Oriented Nanoscale Films of Metal–Organic Frameworks By Room-Temperature Gel-Layer Synthesis.* Angewandte Chemie International Edition, 2010. **49**(40): p. 7225-7228.

29.   Pachfule, P., et al., *Solvothermal synthesis, structure, and properties of metal organic framework isomers derived from a partially fluorinated link.* Crystal Growth & Design, 2011. **11**(4): p. 1215-1222.

30.   Forster, P.M., N. Stock, and A.K. Cheetham, *A High-Throughput Investigation of the Role of pH, Temperature, Concentration, and Time on the Synthesis of Hybrid Inorganic–Organic Materials.* Angewandte Chemie International Edition, 2005. **44**(46): p. 7608-7611.

31.   Hao, S.Y., et al., *Structures, luminescence and photocatalytic properties of two nanostructured cadmium (II) coordination polymers synthesized by sonochemical process.* Ultrasonics sonochemistry, 2018. **40**: p. 68-77.

32.   Dey, C., et al., *Crystalline metal-organic frameworks (MOFs): synthesis, structure and function.* Acta Crystallographica Section B: Structural Science, Crystal Engineering and Materials, 2014. **70**(1): p. 3-10.

33.   Hao, S.Y., X.G. Ma, and G.H. Cui, *Ultrasonic synthesis of two nanostructured cadmium (II) coordination supramolecular polymers: Solvent influence, luminescence and photocatalytic properties.* Ultrasonics sonochemistry, 2017. **37**: p. 414-423.

34.   Jung, D.-W., et al., *Facile synthesis of MOF-177 by a sonochemical method using 1-methyl-2-pyrrolidinone as a solvent.* Dalton Transactions, 2010. **39**(11): p. 2883-2887.

35. Sindoro, M., et al., *Colloidal-sized metal–organic frameworks: synthesis and applications.* Accounts of chemical research, 2013. **47**(2): p. 459-469.

36. Kim, J., et al., *Control of catenation in CuTATB-n metal–organic frameworks by sonochemical synthesis and its effect on CO 2 adsorption.* Journal of Materials Chemistry, 2011. **21**(9): p. 3070-3076.

37. Li, J., et al., *Zinc hydroxide nanostrands: unique precursors for synthesis of ZIF-8 thin membranes exhibiting high size-sieving ability for gas separation.* CrystEngComm, 2014. **16**(42): p. 9788-9791.

38. ASTM, D., *3359-02: standard test methods for measuring adhesion by tape test.* ASTM International, West Conshohocken, PA, 2002.

39. Yoo, Y. and H.-K. Jeong, *Rapid fabrication of metal organic framework thin films using microwave-induced thermal deposition.* Chemical communications, 2008(21): p. 2441-2443.

40. Ji, H., et al., *Direct in Situ Conversion of Metals into Metal–Organic Frameworks: A Strategy for the Rapid Growth of MOF Films on Metal Substrates.* ACS Applied Materials & Interfaces, 2016. **8**(47): p. 32414-32420.

41. Zacher, D., et al., *Deposition of microcrystalline [Cu 3 (btc) 2] and [Zn 2 (bdc) 2 (dabco)] at alumina and silica surfaces modified with patterned self assembled organic monolayers: evidence of surface selective and oriented growth.* Journal of Materials Chemistry, 2007. **17**(27): p. 2785-2792.

42. Okada, K., et al., *Copper Conversion into Cu (OH) 2 Nanotubes for Positioning Cu3 (BTC) 2 MOF Crystals: Controlling the Growth on Flat Plates, 3D Architectures, and as Patterns.* Advanced Functional Materials, 2014. **24**(14): p. 1969-1977.

43. Li, Z.-Q., et al., *Ultrasonic synthesis of the microporous metal–organic framework Cu 3 (BTC) 2 at ambient temperature and pressure: an efficient and environmentally friendly method.* Materials Letters, 2009. **63**(1): p. 78-80.

44. Singh, D.P., A.K. Ojha, and O.N. Srivastava, *Synthesis of different Cu (OH) 2 and CuO (nanowires, rectangles, seed-, belt-, and sheetlike) nanostructures by simple wet chemical route.* The Journal of Physical Chemistry C, 2009. **113**(9): p. 3409-3418.

45. Wang, M., et al., *Rapid room-temperature synthesis of nanosheet-assembled ZnO mesocrystals with excellent photocatalytic activity.* CrystEngComm, 2013. **15**(4): p. 754-763.

46. Top, A. and H. Çetinkaya, *Zinc oxide and zinc hydroxide formation via aqueous precipitation: effect of the preparation route and lysozyme addition.* Materials Chemistry and Physics, 2015. **167**: p. 77-87.

47. Tian, H., et al., *Zeolitic imidazolate framework coated ZnO Nanorods as molecular sieving to improve selectivity of formaldehyde gas sensor.* ACS Sensors, 2015. **1**(3): p. 243-250.

48. Cui, J.-W., et al., *Photoluminescence, electrochemical behavior and photocatalytic activities of cobalt (II) coordination polymer nanostructures synthesized by sonochemical process.* Ultrasonics sonochemistry, 2017. **39**: p. 837-844.

49. Yim, C. and S. Jeon, *Direct synthesis of Cu-BDC frameworks on a quartz crystal microresonator and their application to studies of n-hexane adsorption.* RSC Advances, 2015. **5**(83): p. 67454-67458.

50. Chernikova, V., O. Shekhah, and M. Eddaoudi, *Advanced Fabrication Method for the Preparation of MOF Thin Films: Liquid-Phase Epitaxy Approach Meets Spin Coating Method.* ACS Applied Materials & Interfaces, 2016. **8**(31): p. 20459-20464.

51. McCarthy, M.C., et al., *Synthesis of zeolitic imidazolate framework films and membranes with controlled microstructures.* Langmuir, 2010. **26**(18): p. 14636-14641.

52. Chen, B., et al., *Zeolitic imidazolate framework materials: recent progress in synthesis and applications.* Journal of Materials Chemistry A, 2014. **2**(40): p. 16811-16831.

53. Bux, H., et al., *Zeolitic imidazolate framework membrane with molecular sieving properties by microwave-assisted solvothermal synthesis.* Journal of the American Chemical Society, 2009. **131**(44): p. 16000-16001.

54. Makinson, J., et al., *X-ray diffraction signatures of defects in nanocrystalline materials.* Advances in X-ray Analysis, 2000. **42**: p. 407-411.

55.   Liu, Y., et al., *Synthesis of continuous MOF-5 membranes on porous α-alumina substrates.* Microporous and Mesoporous Materials, 2009. **118**(1): p. 296-301.

56.   Heinke, L., et al., *Surface-mounted metal-organic frameworks for applications in sensing and separation.* Microporous and Mesoporous Materials, 2015. **216**: p. 200-215.

List of Figures

Figure 1. Schematic illustration of the two-step method for the different thin MOF films fabrication.

Figure 2. SEM images of (a) $Cu(OH)_2$ nanowires and (b) $Zn(OH)_2$ nanostrands, after metal surface oxidation.

Figure 3. XRD patterns of (a) Cu-clad (black) and $Cu(OH)_2$ nanowires on Cu-clad substrate (red), and (b) Zn strip (black) and $Zn(OH)_2$ nanostrands on Zn strip substrate (red).

Figure 4. SEM images of Cu-BTC with 0.5 mM BTC under ultrasonic irradiation for (a) 5 min resulting in an average diameter, d, of 380 nm ± 39 nm; (b) 15 min, d = 594 nm ± 27 nm; (c) 30 min, d = 652 nm ± 33 nm; (d) 60 min, d = 672 nm ± 34 nm. The second row shows SEM images of Cu-BDC with 1 mM BDC under ultrasonic irradiation for (e) 5 min resulting in an average length, l, of 84 nm ± 12 nm; (f) 15 min, l = 152 nm ± 20 nm; (g) 30 min, l = 249 nm ± 6 nm; (h) 60 min, l = 282 nm ± 10 nm. The average sizes and standard deviations are determined from the SEM image analysis.

Figure 5. XRD patterns of (a) Cu-BTC film with 0.5 mM BTC, and (b) Cu-BDC film with 1 mM BDC, synthesized at different ultrasonic irradiation times: 5 min (black), 15 min (red), 30 min (blue), and 60 min (magenta).

Figure 6. SEM images of ZIF-8 with 0.1 mM 2-MIM under ultrasonic irradiation for (a) 5 min resulting in an average diameter, d, of 500 nm ± 39 nm; (b) 15 min, d = 713 nm ± 18 nm; (c) 30 min, d = 1762 nm ± 17 nm; (d) 60 min, d = 1922 nm ± 12 nm. The second row shows SEM images of MOF-5 with 1 mM BDC under ultrasonic irradiation for (e) 5 min, d = 224 nm ± 8 nm; (f) 15 min, d = 153 nm ± 18 nm; (g) 30 min, d = 111 nm ± 10 nm; (h) 60 min, d = 113 nm ± 5 nm. The average sizes and standard deviations are determined from the SEM image analysis.

Figure 7. XRD patterns of (a) ZIF-8 film with 0.1 mM 2-MIM, and (b) MOF-5 film with 1 mM BDC, synthesized at different ultrasonic irradiation times: 5 min (black), 15 min (red), 30 min (blue), and 60 min (magenta).

Figure 8. XRD patterns of (a) Cu-BTC film, (b) Cu-BDC film, (c) ZIF-8 film, and (d) MOF-5 film at different organic ligand concentrations.

Figure 9. SEM images of Cu-BTC, Cu-BDC, ZIF-8, and MOF-5 films taken after sonication for 5, 10, 30, and 60 min, from left to right.

Figure 10. Nyquist plots of ZIF-8 film sensor exposed to various concentrations of methane diluted in nitrogen.

Oxidation

Cu clad → Cu(OH)$_2$ nanowires

Ultrasonic bath

Cu-BTC

Cu-BDC

Oxidation

Zn Strips → Zn(OH)$_2$ nanostrands

Ultrasonic bath

MOF-5

ZIF-8
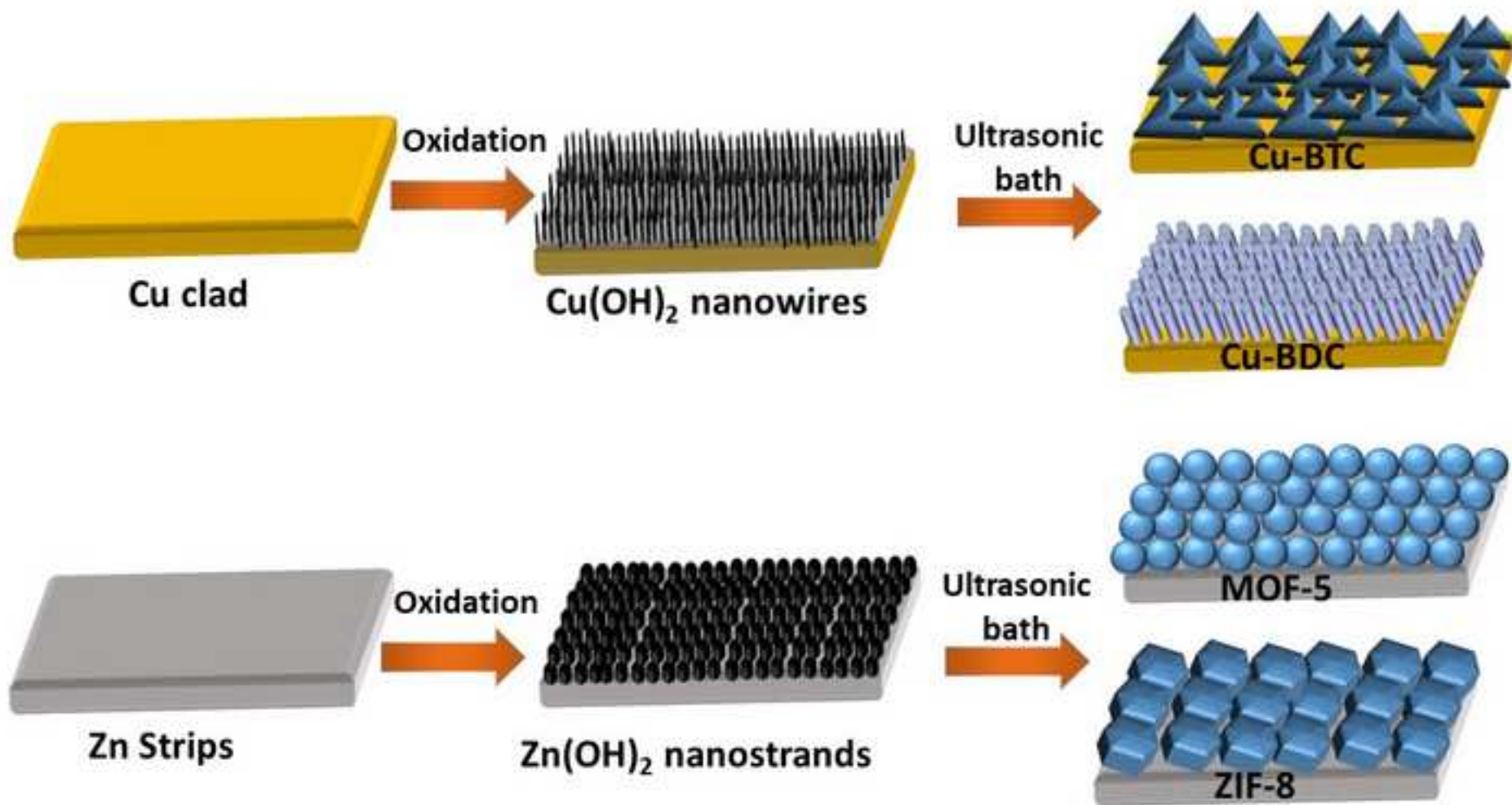
Figure 2
[Click here to download high resolution image](#)
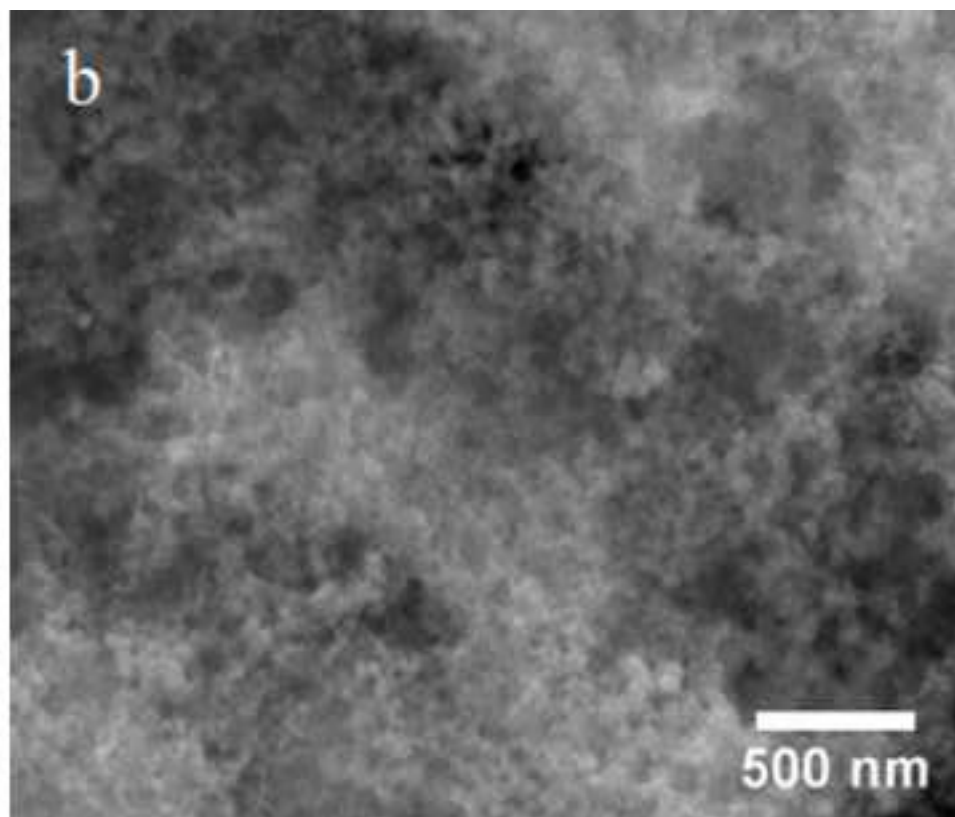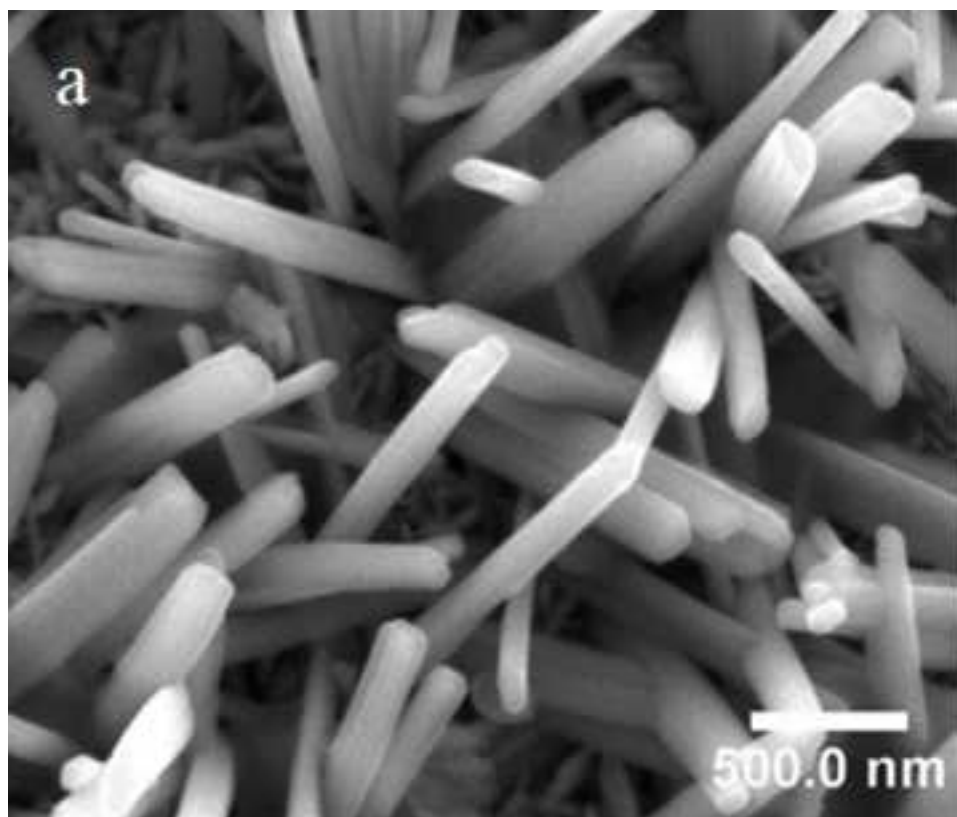
Figure 3
[Click here to download high resolution image](#)
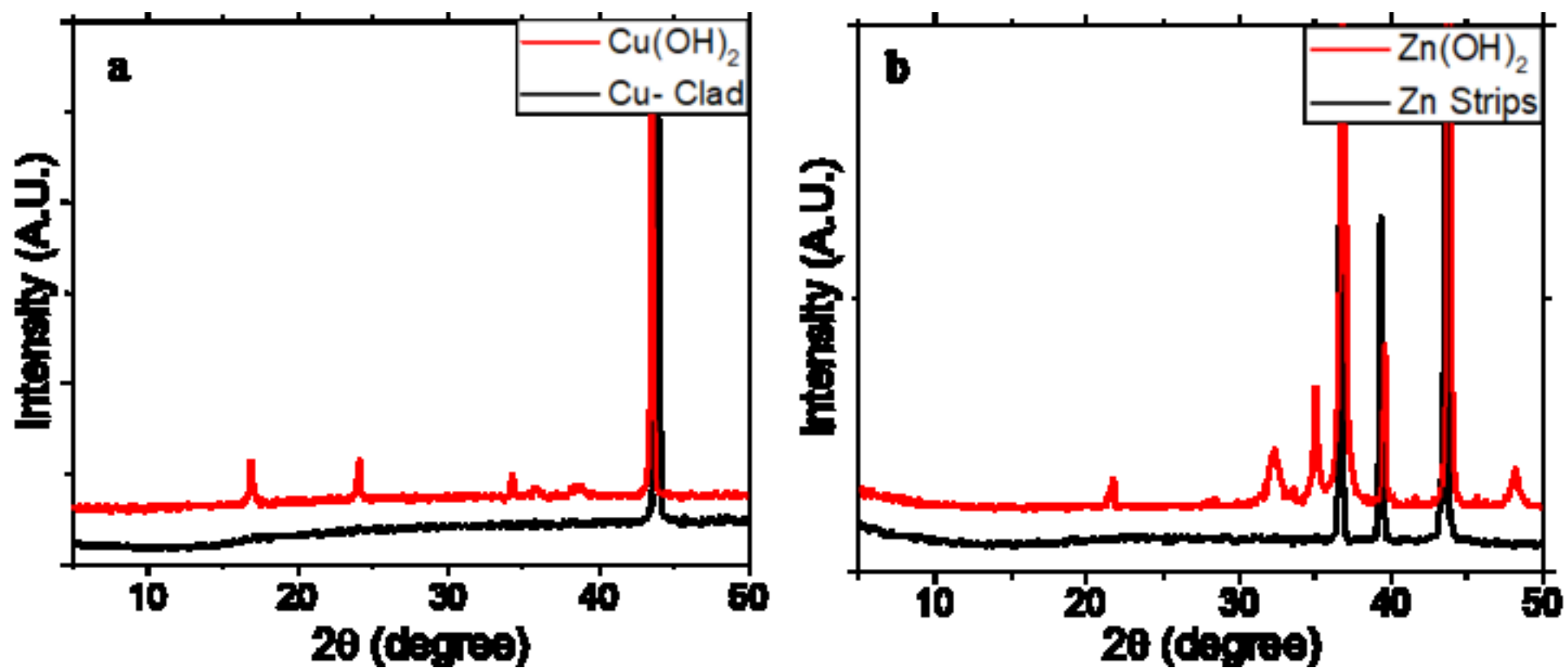
Figure 4
[Click here to download high resolution image](#)
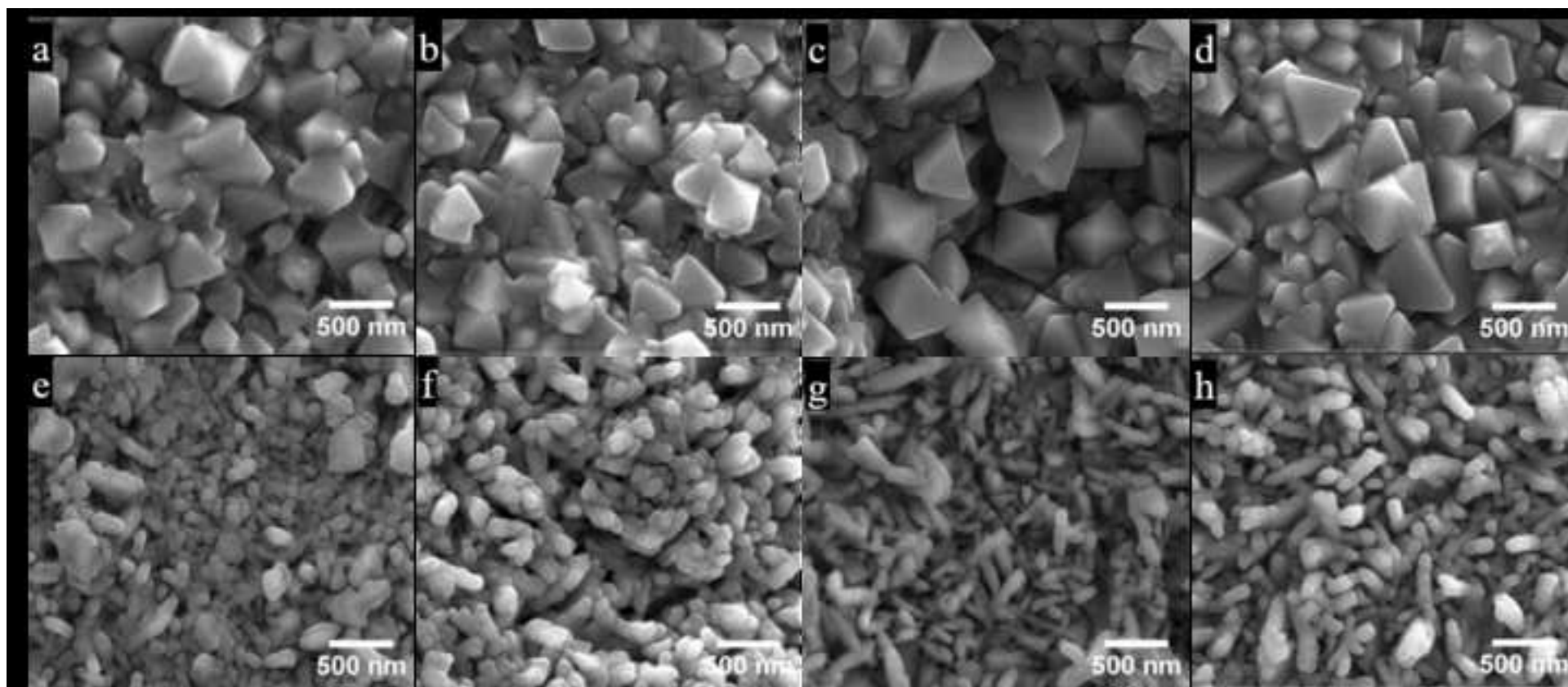
Figure 5
Click here to download high resolution image
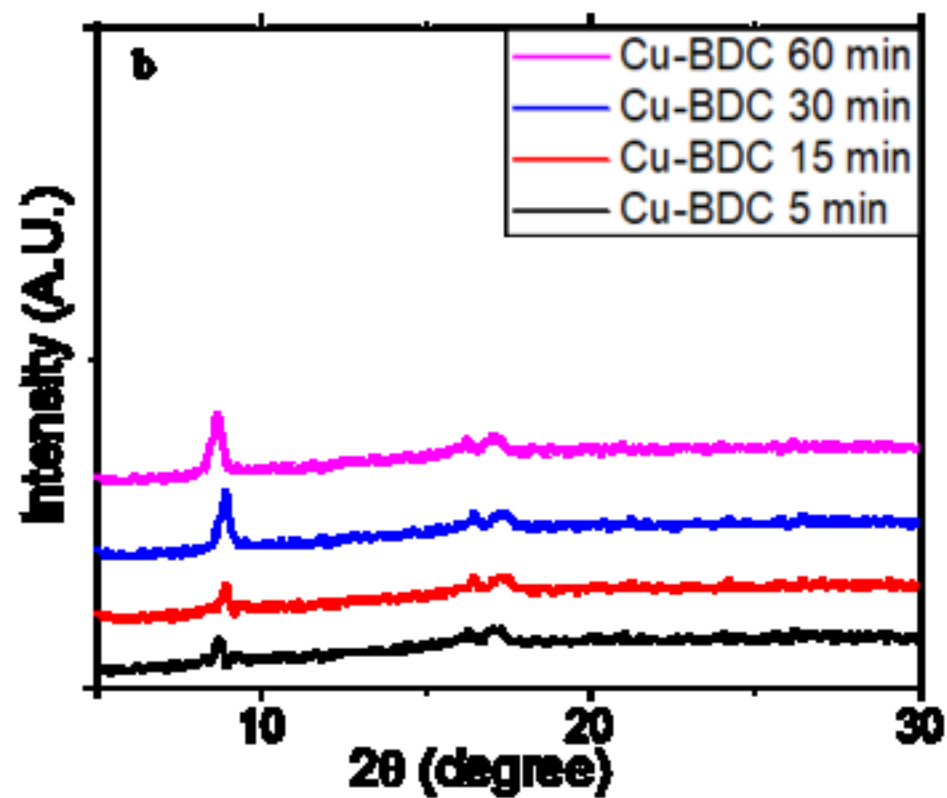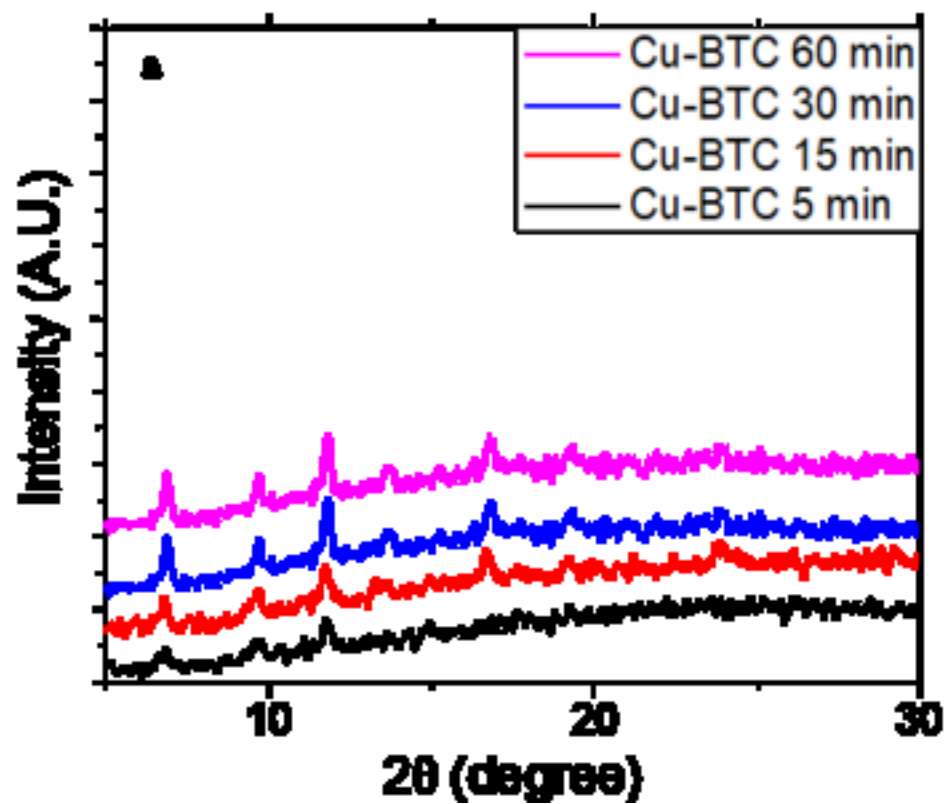
Figure 6
[Click here to download high resolution image](#)
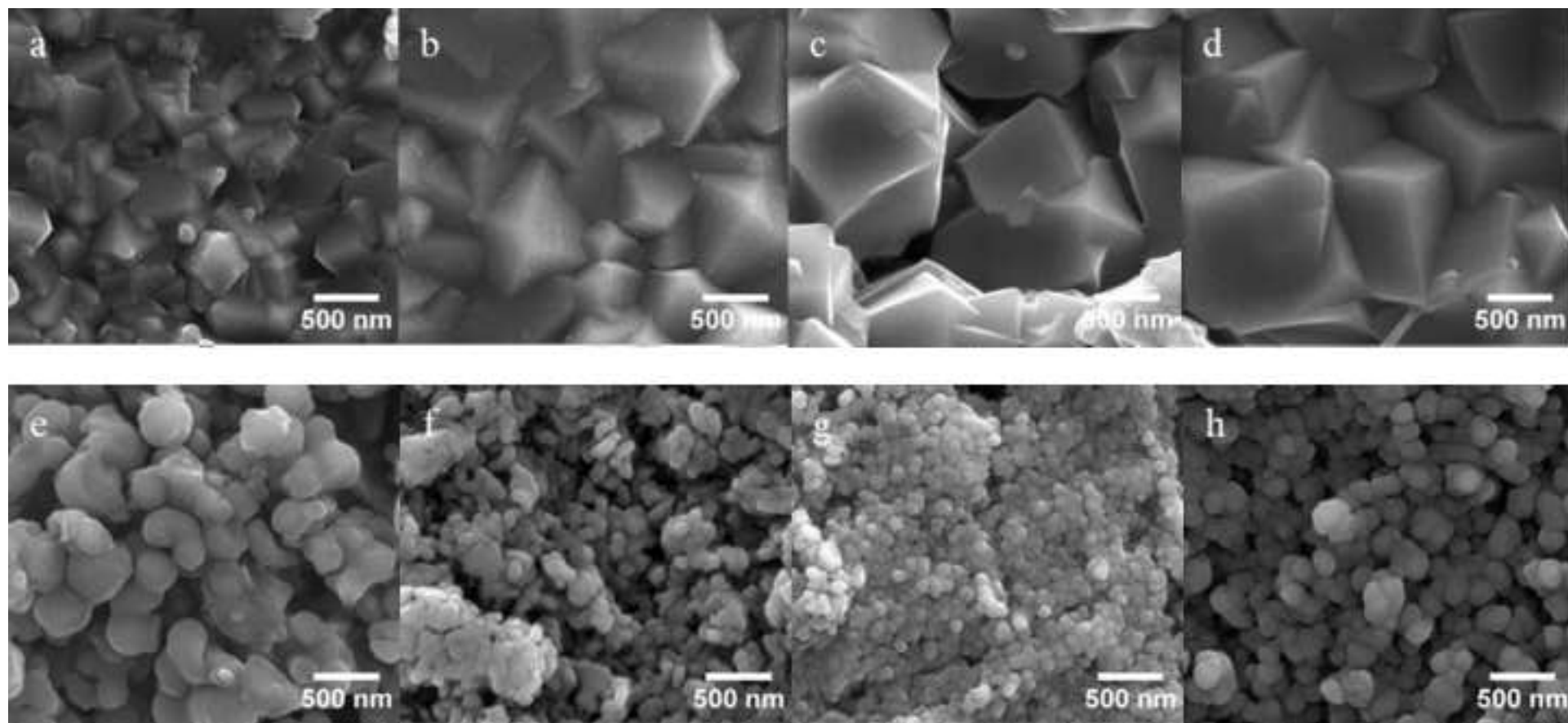
Figure 7
[Click here to download high resolution image](#)
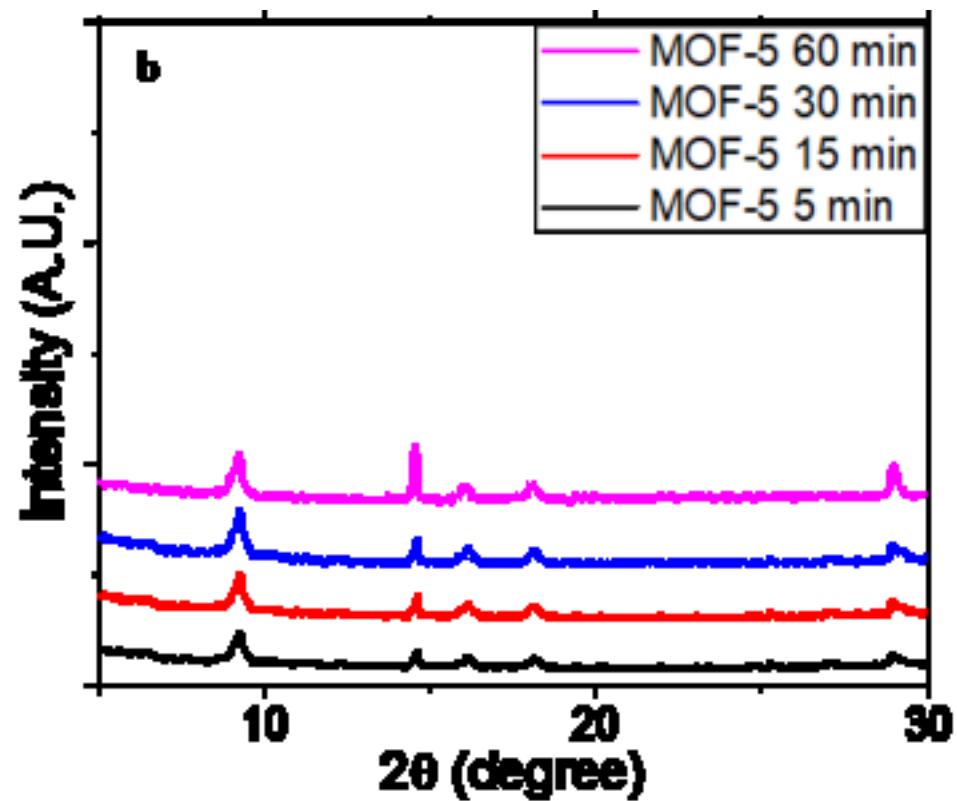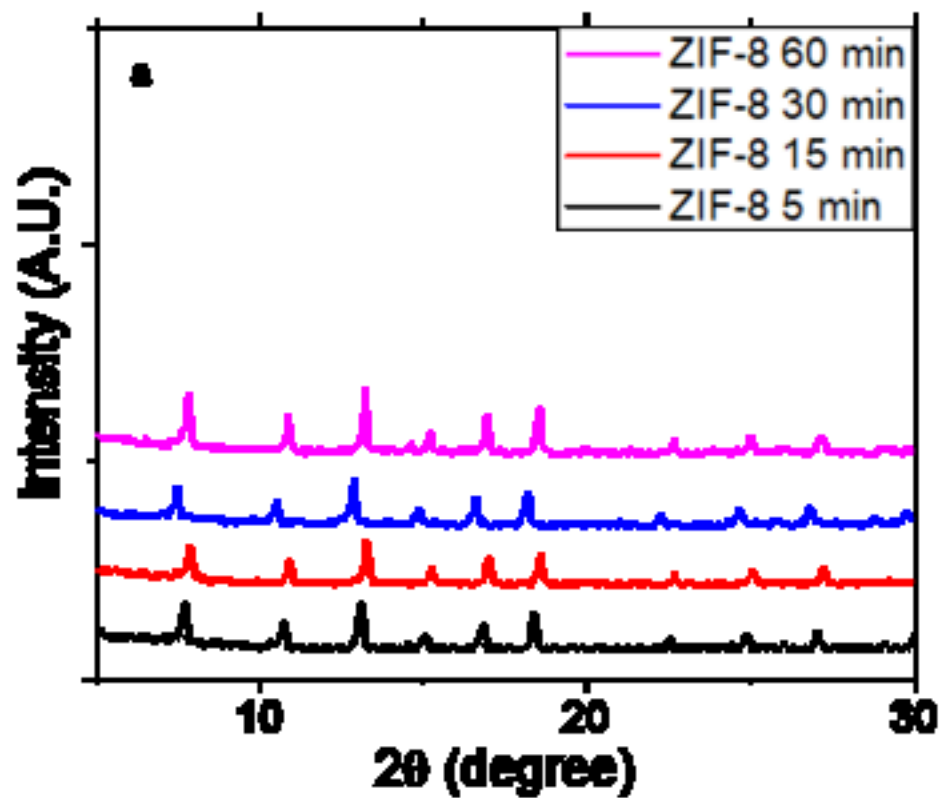
Figure 8
[Click here to download high resolution image](#)
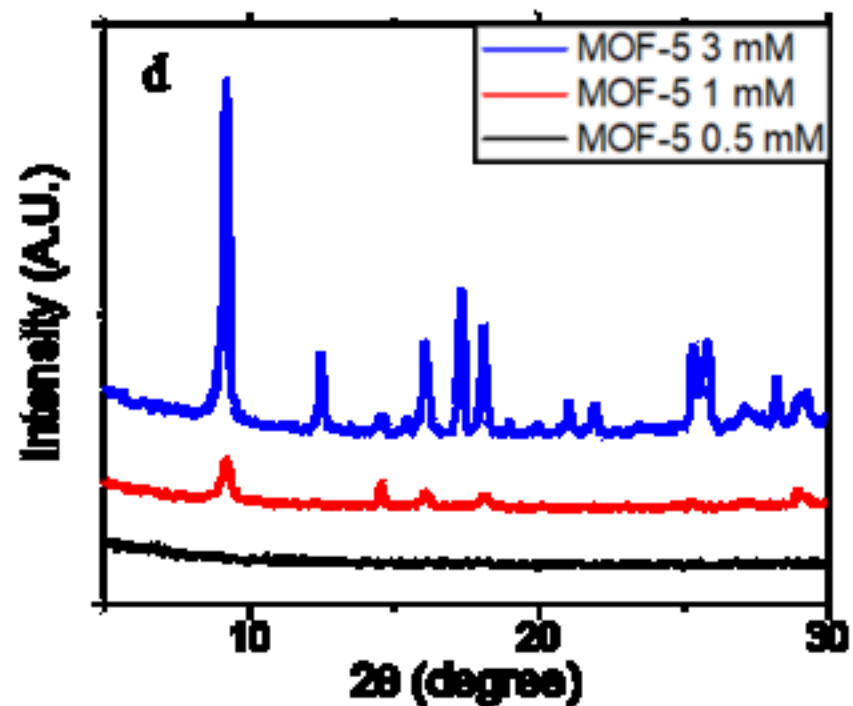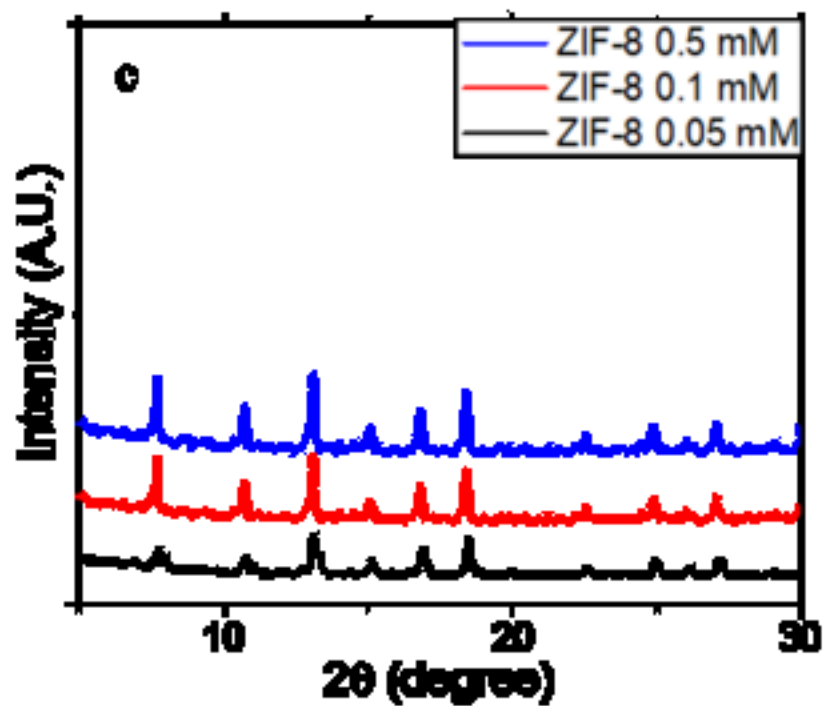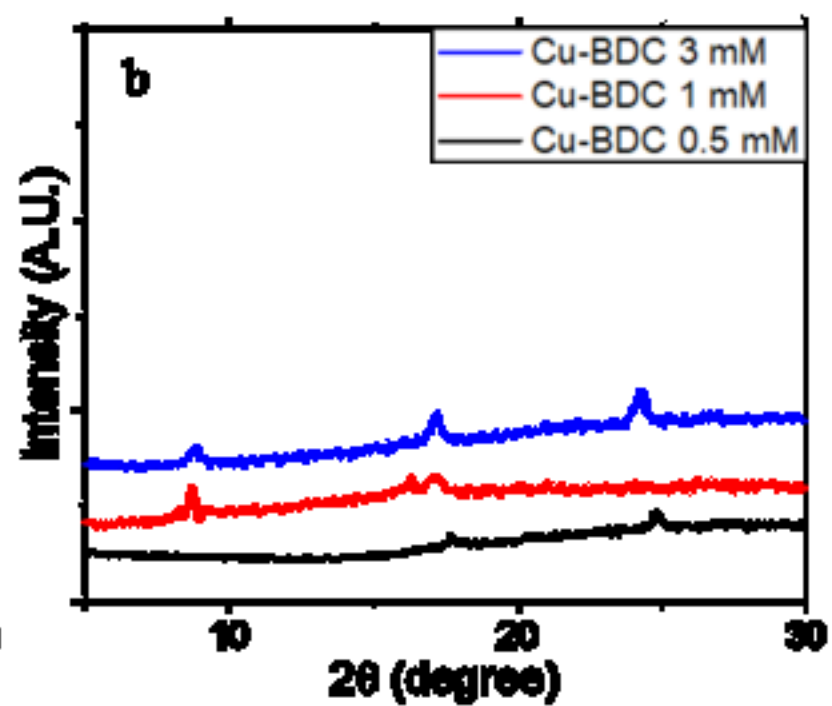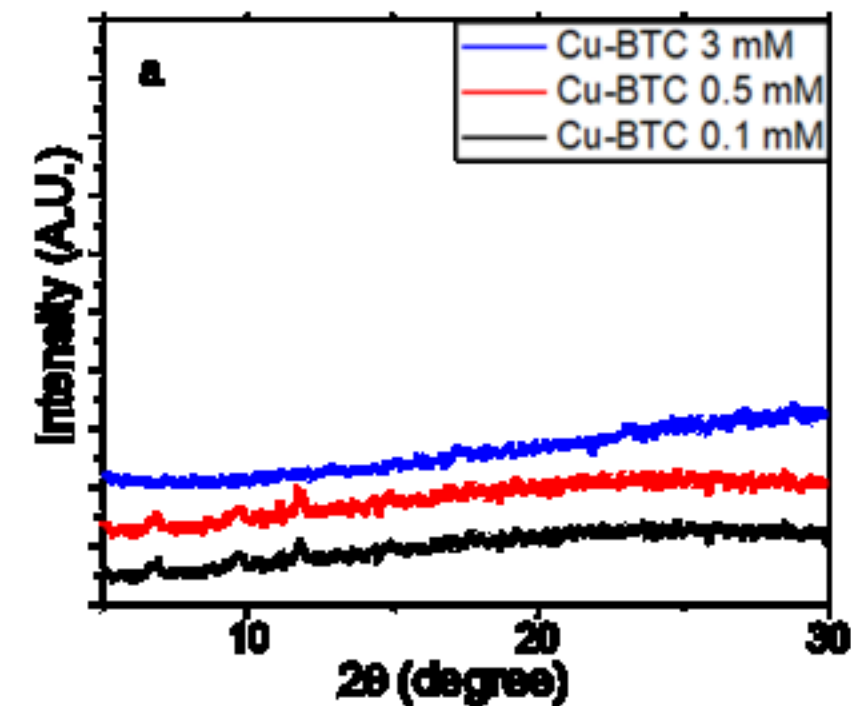
Figure 9
[Click here to download high resolution image](#)